Plasmonic multiple exciton generation

Jiantao Kong,[1] Xueyuan Wu,[1] Xin Wang,[2,3] Michael J. Naughton,[1,2] and Krzysztof Kempa[1,4]

[1]*Department of Physics, Boston College, Chestnut Hill, Massachusetts 02467, USA*

[2]*International Academy of Optoelectronics at Zhaoqing, South China Normal University, Zhaoqing, Guangdong Province 526238, China*

[3]*National Center for International Research on Green Optoelectronics, South China Normal University,*
Guangzhou, Guangdong Province 510631, China

[4]*Academy of Advanced Optoelectronics, South China Normal University, Guangzhou, Guangdong Province 510631, China*

We show that biexciton formation can be highly efficient in a solar cell whose semiconductor absorber is filled with an array of metallic nanoparticles having plasmonic resonances tuned to the semiconductor gap energy. This process can be viewed as a plasmon-enhanced multiple exciton generation, with the resulting cell efficiency exceeding the Shockley-Queisser limit. We demonstrate via theory and simulations that the efficiency of the process increases with decreasing semiconductor gap size, and illustrate such by considering in detail three systems with gradually decreasing gap size: GaAs, Si, and Ge.

I. INTRODUCTION

Electrons or holes in semiconductors, excited into their respective conduction and valence bands away from the thermal equilibrium distributions, are referred to as "hot." Effects of hot electrons have been studied and utilized for more than half a century in a variety of electronic devices, from Gunn diodes to integrated circuits [1–10]. In conventional solar cells, hot electrons rapidly and irreversibly lose their excess or hot energy to phonons (heat), which leads to the Shockley-Queisser limit for single junction cell efficiency [11]. The amount of the energy lost to heat in a conventional solar cell actually exceeds that harvested in the form of usable electricity. For example, commercially available, high efficiency crystalline silicon solar cells convert 20%−25% of absorbed sunlight into electricity, but more than 30% into heat via hot electrons. Many concepts have been proposed to harvest or convert this hot electron energy into usable form, but none have been experimentally verified or demonstrated to date [11]. One of the seminal concepts proposed for so called third-generation solar photovoltaics (PV) involves harvesting the excess energy of these hot electrons before it is dissipated as heat [12], with theoretical efficiency limits of over 60%. This is posited to be achievable by first somehow eliminating the phonon scattering in the active region, and then extracting the hot electrons through narrow band energy filters at absorber-electrode contacts, assuring isentropic cooling. However, this is far from a trivial proposition, and no successful solar cell based on this idea has been developed. While early investigations found some evidence for hot electron injection into an electrolyte [13], and the hot electron contribution to the photovoltage was recently demonstrated [14], there remains limited experimental evidence of improved photovoltaic performance via hot electrons, despite many decades of research.

In another important scheme to recover the hot electron energy, it was envisioned that a single photon in a solar cell could generate two or more electron-hole pairs (physically separated excitons), instead of the canonical single pair. This is the multi-exciton generation (MEG) concept [15–17], known to be vanishingly small in bulk materials in the frequency range of interest to photovoltaics. It has been demonstrated in laser spectroscopic [16,17] and photocurrent [18] studies that, in semiconductor nanoparticles (NPs), it can become significant.

Recently, some of the present authors proposed a plasmonic, third-generation PV scheme by providing an efficient energy-dissipation channel into plasmons in an adjacent or embedded plasmonic structure [19]. In this scheme, the hot electron free energy remains reversibly "protected" in a collective electronic degree of freedom. This hot electron plasmon protection (HELPP) mechanism, which relies on electron-plasmon scattering occurring on a time scale sufficiently smaller than phonon emission by either plasmons or hot electrons, was theoretically supported by a simple model calculation [19]. Here, we describe a way to combine the HELPP concept with MEG, a process which can be viewed as plasmon-enhanced multiple exciton generation (PMEG).

II. METHODS

The MEG theory often breaks the process into two steps. First, an incoming photon excites a single exciton, with hot carriers participating and second, this exciton, before emitting phonons, decays into multiple excitons via Coulomb scattering [20]. Instead of employing Fermi's golden rule to estimate the decay rate of excitons (hot electrons and holes) to biexcitons, we calculate the hot electron scattering rate exactly, including secondary excitons as a part of the single particle excitation continuum. The scattering rate of an electron in a semiconductor matrix from a state $E_{\mathbf{k}}$ to all other states $E_{\mathbf{k}\pm\mathbf{q}}$, due to single particle and collective (plasmon) excitations (with wave vectors $\mathbf{q}$), is given in the

random-phase approximation (RPA) [21] by

$$\gamma_{\text{el-el}} = \frac{2}{\hbar} \int \frac{d\mathbf{q}}{(2\pi)^3} V_q [n_B(E_{\mathbf{k}} - E_{\mathbf{k+q}}) - n_F(-E_{\mathbf{k+q}} + \mu)]$$

$$\times \text{Im}\left[\varepsilon\left(q, \frac{E_{\mathbf{k+q}} - E_{\mathbf{k}}}{\hbar}\right)^{-1}\right], \quad (1)$$

where n_B and n_F are the Bose-Einstein and Fermi-Dirac distribution functions, respectively, μ is the chemical potential, $\varepsilon(q,\omega)$ is the effective longitudinal dielectric function of the medium, and V_q is the bare Coulomb interaction. Clearly, this calculation requires knowledge of the effective dielectric function of a given structure. In a simple, single Lorentzian approximation, the dielectric function can be written as [22]

$$\varepsilon(\omega) = \varepsilon_b + \frac{\omega_p^2}{\omega_r^2 - \omega(\omega + i\gamma)}, \quad (2)$$

which, for $\gamma \to 0^+$ and $\omega_r^2 \gg \omega_p^2$, when inserted into Eq. (1), leads to a simple formula [23]

$$\gamma_{\text{el-el}} \approx \frac{\sqrt{2E_k/m}}{2a^*} f\left(\frac{E_k}{\hbar\omega_r}\right) \Theta\left(\frac{E_k}{\hbar\omega_r} - 1\right), \quad (3)$$

where the renormalized Bohr radius is $a^* = a_B \varepsilon_b^2 (\omega_r/\omega_p)^2$, and the auxiliary function $f(x) = \frac{2}{x} \ln(\sqrt{x} + \sqrt{x-1})$ varies slowly for $x > 1.5$. Equation (3) can be used as guidance for more rigorous calculations/simulations, and it shows, as expected, that the scattering vanishes for $E_k < \hbar\omega_r$, and also that it increases rapidly with increasing plasmonic oscillator strength ω_p.

III. RESULTS

Consider now a PV absorber filled with an array of simple spherical metal NPs (i.e., nanospheres), as depicted in the inset to Fig. 1. We chose the NPs to be in a cubic lattice of period a and the nanosphere diameter $D = a/3$, so that the projected area fraction remains unchanged as we vary a. The relative absorption (per unit volume of the absorber), as simulated in FDTD [24,25] for crystalline GaAs semiconductor and Ag NPs, is shown in Fig. 1, for six values of a.

Figure 1 shows that the frequency of the plasmonic absorption increases with decreasing a, and saturates ~400 THz. This behavior reflects the well-known dispersion relation of a surface plasmon induced on the surface of the metallic sphere; changing the sphere diameter changes an effective surface plasmon quasi-momentum according to the "whispering gallery" mode condition [22,26] $q \approx 2/D$. The plasmonic absorption peak strengths rapidly increases once the peak frequency enters the intersubband transition region above the gap energy of 1.4 eV (~340 THz). In this region, massive generation of interband transitions (i.e., excitons) by decaying hot electrons is also expected, as will be demonstrated below. The absorption spectrum for each value of a is dominated by a single plasmonic resonance, and so one could use Eq. (2) as a simple model of the dielectric function, and then use Eq. (3) to estimate of the scattering rate. For an accurate analysis, we extract the effective dielectric function of the medium by the method described in detail in [26], and then use the exact result from Eq. (1) to obtain the scattering
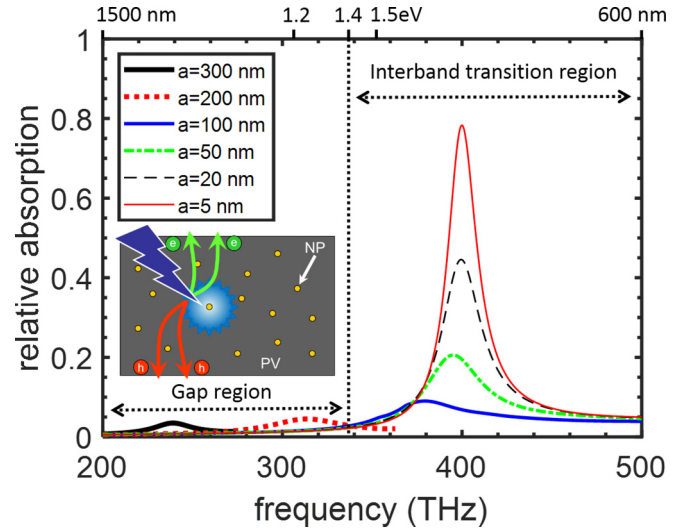

FIG. 1. Relative (per unit volume of the absorber) absorption spectra of GaAs absorber filled with cubic array of Ag NPs (period a, diameter $D = a/3$). Strong plasmonic absorbance is seen around 400 THz. Inset shows basic PMEG scheme: incident high energy photon (dark blue) interacts with NP to establish a surface plasmon, whose strong E field (gradient blue) excites a biexciton, which separates into two electron-hole pairs, which drift/diffuse via an inferred p-n junction. Top axis shows relevant energy and wavelength scales.

rate. The extracted single Lorentzian dielectric functions for $D = 67$ nm and 6.7 nm are shown in Fig. 2. The inset shows the corresponding scattering rates vs. hot electron energy. For the smaller spheres, intersubband transitions are possible (producing secondary excitons), and the scattering rates of hot electrons with energies 2.5 eV and more above the conduction band edge exceed 2×10^{13} s^{-1} (i.e., faster than 50 ps). This rate is larger than the phonon cooling rate in GaAs of
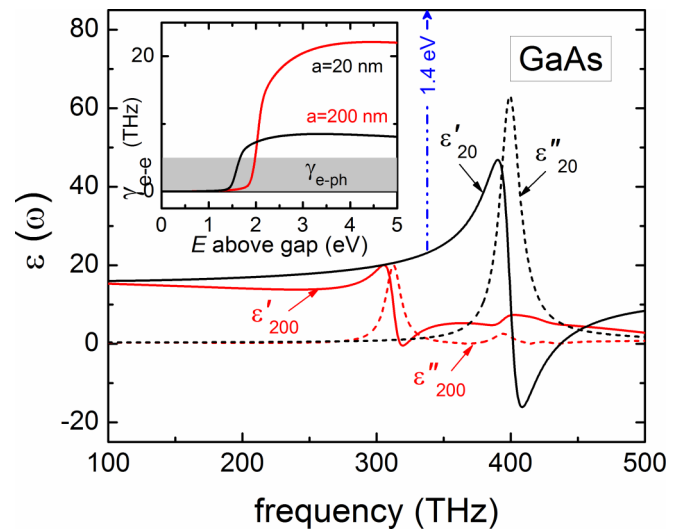

FIG. 2. Extracted effective dielectric function of the GaAs absorber filled with a cubic array of Ag nanospheres (each with diameter $D = a/3$) for two nanosphere sizes $D = 6.7$ nm (black) and $D = 67$ nm (red). The inset shows the corresponding electron-electron scattering rates. The shaded area represents the rates of electron-phonon scattering processes.
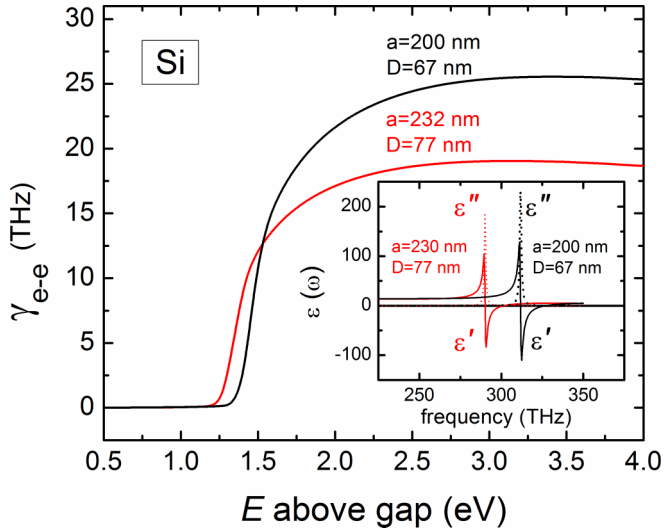
FIG. 3. Calculated electron-electron scattering rates for a crystalline Si absorber filled with a cubic array of Ag nanospheres (of diameter $D = a/3$), with $a = 200$ nm (black curve) and $a = 230$ nm (red curve). The inset shows the corresponding extracted effective dielectric functions, used to obtain the scattering rates.
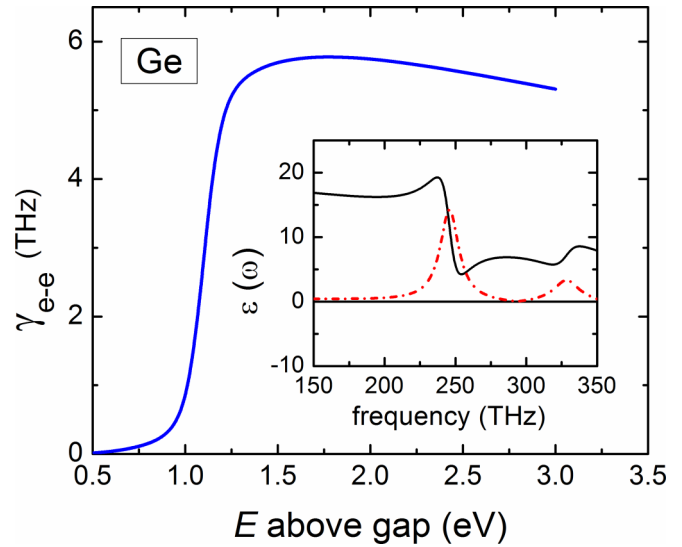

FIG. 4. Calculated electron-electron scattering rates for a Ge absorber filled with a cubic array of Ag nanospheres (each with diameter $D = a/3 = 67$ nm). The inset shows the corresponding extracted effective dielectric function, used to obtain the scattering rates.

$\sim 0.5 \times 10^{13}$ s^{-1} (i.e., 200 ps) [27]. This is the rate at which the hot electrons cool to the bottom of the conduction band, which requires many electron-phonon scattering events; the energy of a single phonon is only ~ 36 meV, such that more than 50 scattering events are needed to completely cool a hot electron with energy 2 eV. The shaded area in the inset in Fig. 2 shows an estimated cooling rate. For larger spheres ($D = 67$ nm), with resonances below the energy gap, no secondary excitons are generated, only plasmons at a smaller rate.

As the efficiency of PMEG diminishes with increasing gap size, only hot electrons with energy greater than the gap can generate secondary excitons. In fact, GaAs is not an optimal material for PMEG solar cells. The maximum value of the hot electron energy generated by AM1.5 solar radiation (as measured from the top of the valence band) is about 3.4 eV [28], and so we estimate that in GaAs, the hot electrons reach only about 3.4 eV–1.4 eV = 2 eV into the conduction band. However, Fig. 2 shows that significant (exceeding the phonon scattering rate) plasmon generation occurs for hot electrons with energy >2 eV, such that only a small fraction of photogenerated hot electrons can generate secondary excitons. Nevertheless, GaAs is a good material to demonstrate the PMEG effect by using laser illumination.

Next, we investigated crystalline Si. Employing the same procedure as for GaAs, we obtained the result shown in Fig. 3. The scattering rates are shown in the main part of the figure, for two NP diameters, $D = 67$ and 76 nm. In this case, we have the solar radiation-induced hot electron bandwidth equal to 3.4 eV–1.1 eV = 2.3 eV. For the larger diameter sphere, we obtain a significant scattering rate ($\sim 1.5 \times 10^{13}$ sec^{-1}) already for 1.3 eV, which exceeds that of the electron-phonon cooling rate ($< 10^{13}$ sec^{-1}). Thus, in this case, a reasonably large portion of the hot electron distribution, $\sim 43\%$, is available for PMEG recovery. Thus, crystalline

Si is a viable material for both PMEG demonstration and a PMEG solar cell.

Semiconductors with even smaller gaps, such as crystalline c-Ge (0.68 eV) or amorphous a-Ge (0.83 eV), should further improve the efficiency of PMEG. As an example, we consider c-Ge in Fig. 4, for NPs with $D = 33.3$ nm. The scattering rate has a maximum near 1.5 eV, representing the PMEG. Since in this case the range of hot electrons induced by a 1-sun illumination is 3.4 eV – 0.68 eV ~ 2.7 eV (as measured from the bottom of the conduction band), a large fraction of hot electrons (more than 50%), with energies ranging from 1.3 to 2.7 eV, can produce the secondary electrons. The electron-phonon scattering rate in Ge is $\sim 10^{14}$ sec^{-1} [29], and the corresponding cooling rate (in view of the single phonon emission energy of ~ 20 meV [30]) is $\sim 10^{12}$ sec^{-1}, much lower than the electron-electron scattering rate. Thus, we can conclude that c-Ge could be used as a practical platform for PMEG cells.

Figure 5 shows that there is a relative insensitivity of our results to NP spacing a and NP size (e.g., sphere diameter D) in a quite wide parameter range. For example, when a is varied from 100 to 300 nm for fixed $D = 67$ nm, or from 100 to 400 nm for fixed $D = 50$ nm, the resonance frequency varies only by about 10%. At fixed $a = 400$ nm, more pronounced but still quite moderate changes ($\sim 20\%$) occur when the NP diameter D varies from 50 nm to 200 nm. These are expected from the known diameter insensitivity of the Mie resonance of spherical particles (see Ref. [22]). Figure 5 suggests that a similar approximate insensitivity should hold for other geometries (including random) with similar inter-NP spacings, and similar NP diameters. Thus, the cubic lattice of spherical NPs used in this study is a good representative model of the proposed systems. This analysis suggests also that the tunability of the resonances will be achieved mainly by changing the *intra*-NP features in addition
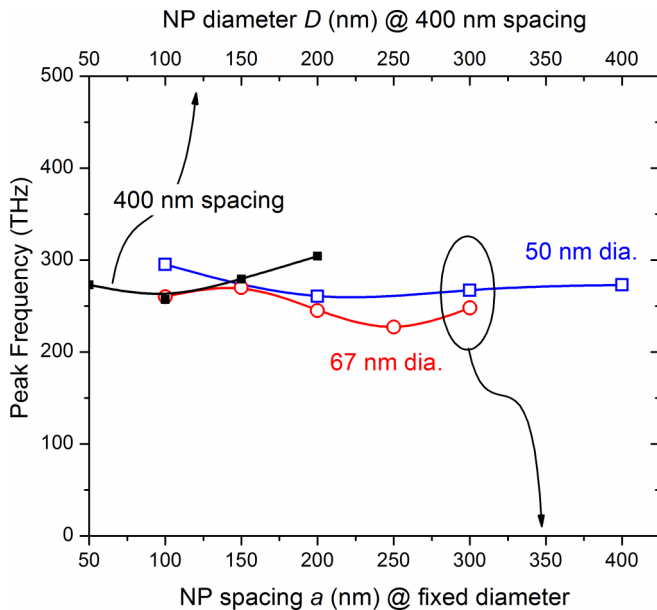
FIG. 5. Peak plasmonic resonance frequency vs spacing *a* and size *D*, for cubic arrays of Ag nanospheres immersed in a Ge absorber.

to size, such as shape (cube, star, etc.) and sub-structure (e.g., core-shell).

IV. DISCUSSION

Embedding plasmonic NPs into crystalline semiconductors is challenging, but possible. Most promising are crystalline NPs of silicides, which are plasmonic with plasma energies in the 3 eV range [31], and so similar to Ag or Au. Most importantly, silicides are nearly lattice matched to Si, so they can be epitaxially grown on Si [32], and vice versa [33]. Many of the silicide NPs are also compatible with Ge. Another emerging technology is NP implantation, which allows deposition of NP growth seeds into semiconductors by ion implantation, and subsequent NP growth from those seeds during annealing, which restores crystalline structure [34]. Wet chemistry-processed semiconductors, such as perovskites, are perhaps most amenable to implementation, as NP embedding can be achieved by simply mixing the NPs with the semiconductor precursor solution. Embedding NPs into amorphous semiconductors processed by PECVD (a-Si and a-Ge) can be also obtained relatively easily by the layer-by-layer processing [35], or co-sputtering of a metal and semiconductor, followed by thermal processing [36].

In conclusion, we show that photoexcitation of two-pair bi-excitons can be protected against phonon emission, and therefore be a statistically likely event, if the semiconductor is filled with metallic NPs having plasmonic resonance tuned to the semiconductor gap energy. The bi-exciton formation process then results from a rapid sequence of two events: (i) initial exciton generation by the incoming photon, and (ii) the second exciton generation by the plasmon-stimulated hot electron's decay. This process can be viewed as plasmon-enhanced multiple exciton generation, PMEG. We demonstrate that the intra-NP physics dominates the resonance tuning which, on one hand, makes our conclusions approximately valid for a range of periodic or aperiodic NP arrangements and, on the other, allows for a small inter-NP spacing, which increase the volume fraction of the affected semiconductor outside the NPs. The universality of this effect provides a new paradigm in the development of ultrahigh efficiency solar cells, beyond the Shockley-Queisser limit. We also demonstrated that PMEG solar cells benefit from smaller gap semiconductors, and considered in detail three systems: large gap GaAs, intermediate gap c-Si and low gap Ge. While the first can be used only to demonstrate the PMEG process, the latter two could provide a possible platform for PMEG solar cells.

[1] J. B. Gunn, Microwave oscillation of current in III-V semiconductors, Solid State Commun. **1**, 88 (1963).

[2] H. Kroemer, Theory of the Gunn effect, Proc. IEEE **52**, 1736 (1964).

[3] D. Frohman-Bentchkowsky, Memory behavior in a floating-gate avalanche-injection MOS (FAMOS) structure, Appl. Phys. Lett. **18**, 332 (1971).

[4] M. Heiblum, M. I. Nathan, D. C. Thomas, and C. M. Knoedler, Direct Observation of Ballistic Transport in GaAs, Phys. Rev. Lett. **55**, 2200 (1985).

[5] C. Rauch, G. Strasser, K. Unterrainer, W. Boxleitner, K. Kempa, and E. Gornik, Ballistic electron spectroscopy of vertical biased superlattices, Physica E **2**, 282 (1998).

[6] A. Othonos, Probing ultrafast carrier and phonon dynamics in semiconductors, J. Appl. Phys. **83**, 1789 (1998).

[7] J. R. Goldman and J. A. Prybyla, Ultrafast Dynamics of Laser-Excited Electron Distributions in Silicon, Phys. Rev. Lett. **72**, 1364 (1994).

[8] S. M. Sze, Microwave diodes, in *High-Speed Semiconductor Devices*, edited by S. M. Sze (Wiley, New York, 1990), Chap. 9.

[9] K. M. Kramer and W. N. G. Hitchon, *Semiconductor Devices: A Simulation Approach* (Prentice Hall PTR, Upper Saddle River, New Jersey, 1997).

[10] J. A. Kash and J. C. Tsang, Watching chips work: picosecond hot electron light emission from integrated circuits, J. Cryst. Growth **210**, 318 (2000).

[11] M. A. Green, *Third Generation Photovoltaics: Advanced Solar Energy Conversion* (Springer-Verlag, Berlin, 2006).

[12] R. T. Ross and A. J. Nozik, Efficiency of hot-carrier solar energy converters, J. Appl. Phys. **53**, 3813 (1982).

[13] J. A. Turner and A. J. Nozik, Evidence for hot-electron injection across *p*-GaP/electrolyte junctions, Appl. Phys. Lett. **41**, 101 (1982).

[14] K. Kempa, M. J. Naughton, Z. F. Ren, A. Herczynski, T. Kirkpatrick, J. Rybczynski, and Y. Gao, Hot electron effect in nanoscopically thin photovoltaic junctions, Appl. Phys. Lett. **95**, 233121 (2009).

[15] M. C. Beard, J. M. Luther, O. E. Semonin, and A. J. Nozik, Third generation photovoltaics based on multiple exciton generation in quantum confined semiconductors, Acc. Chem. Res. **46**, 1252 (2013).

[16] R. D. Schaller and V. I. Klimov, High Efficiency Carrier Multiplication in PbSe Nanocrystals: Implications for Solar Energy Conversion, Phys. Rev. Lett. **92**, 186601 (2004).

[17] M. C. Beard, J. M. Luther, and A. J. Nozik, The promise and challenge of nanostructured solar cells, Nat. Nanotechnol. **9**, 951 (2014).

[18] O. E. Semonin, J. M. Luther, S. Choi, H.-Y. Chen, J. Gao, A. J. Nozik, and M. C. Beard, Peak external photocurrent quantum efficiency exceeding 100% via MEG in a quantum dot solar cell, Science **334**, 1530 (2011).

[19] J. Kong, A. H. Rose, C. Yang, J. M. Merlo, M. J. Burns, M. J. Naughton, and K. Kempa, A hot electron plasmon-protected solar cell, Opt. Express **23**, A1087 (2015).

[20] M. Voros, G. Galli, and G. T. Zimanyi, Colloidal nanoparticles for intermediate band solar cells, ACS Nano **9**, 6882 (2015).

[21] G. D. Mahan, *Many-Particle Physics* (Plenum Press, New York, 1981).

[22] Y. Wang, E. Plummer, and K. Kempa, Foundations of plasmonics, Adv. Phys. **60**, 799 (2011).

[23] K. Kempa, Plasmonic protection of the hot-electron energy, Phys. Stat. Solidi RRL **7**, 465 (2013).

[24] A. Taflove and S. C. Hagness, *Computational Electrodynamics: The Finite-Difference Time-Domain Method* (Artech, Norwood, MA, 1995).

[25] CST Microwave Studio, Computer Simulation Technology AG, https://www.cst.com/products/cstmws.

[26] D. R. Smith, S. Schultz, P. Markoš, and C. M. Soukoulis, Determination of effective permittivity and permeability of metamaterials from reflection and transmission coefficients, Phys. Rev. B **65**, 195104 (2002).

[27] M. Bernardi, D. Vigil-Fowler, C. S. Ong, J. B. Neaton, and S. G. Louie, *Ab initio* study of hot electrons in GaAs, Proc. Natl. Acad. Sci. USA **112**, 5291 (2015).

[28] M. Bernardi, D. Vigil-Fowler, J. Lischner, J. B. Neaton, and S. G. Louie, *Ab Initio* Study of Hot Carriers in the First Picosecond After Sunlight Absorption in Silicon, Phys. Rev. Lett. **112**, 257402 (2014).

[29] N. Tandon, J. D. Albrecht, and L. R. Ram-Mohan, Electron-phonon interaction and scattering in Si and Ge: Implications for phonon engineering, J. Appl. Phys. **118**, 045713 (2015).

[30] R. T. Payne, Phonon energies in germanium from phonon-assisted tunneling, Phys. Rev. **139**, A570 (1965).

[31] R. Soref, R. E. Peale, and W. Buchwald, Longwave plasmonics on doped silicon and silicides, Opt. Express **16**, 6507 (2008).

[32] L. J. Chen, Metal silicides: An integral part of microelectronics, JOM **57**, 24 (2005).

[33] J.-Y. Veuillen, Growth of silicon thin films on erbium silicide by solid phase epitaxy, J. Appl. Phys. **75**, 223 (1994).

[34] H. W. Seo, Q. Y. Chen, I. A. Rusakova, Z. H. Zhang, D. Wijesundera, S. W. Yeh, X. M. Wang, L. W. Tu, N. J. Ho, Y. G. Wu, H. X. Zhang, and W. K. Chu, Formation of silver nanoparticles in silicon by metal vapor vacuum arc ion implantation, Nucl. Instrum. Methods Phys. Res. B **292**, 50 (2012).

[35] Y. Zhang, B. Cai, and B. Jia, Ultraviolet plasmonic aluminium nanoparticles for highly efficient light incoupling on silicon solar cells, Nanomaterials **6**, 95 (2016).

[36] R. Sachan, C. Gonzalez, O. Dyck, Y. Wu, H. Garcia, S. J. Pennycook, P. D. Rack, G. Duscher, and R. Kalyanaraman, Enhanced absorption in ultrathin Si by $NiSi_2$ nanoparticles, Nanomater. Energy **2**, 11 (2015).